Adhesion Between Thin Cylindrical Shells With Parallel Axes

Carmel Majidi[1]
Princeton Institute for the Science and Technology of Materials,
Princeton University,
Princeton, NJ 08544
e-mail: cmajidi@princeton.edu

Kai-tak Wan[2]
Associate Professor
Mechanical and Industrial Engineering,
Northeastern University,
Boston, MA 02115
e-mail: ktwan@coe.neu.edu

Energy principles are used to investigate the adhesion of two parallel thin cylindrical shells under external compressive and tensile loads. The total energy of the system is found by adding the strain energy of the deformed cylinder, the potential energy of the external load, and the surface energy of the adhesion interface. The elastic solution is obtained by linear elastic plate theory and a thermodynamic energy balance, and is capable of portraying the measurable quantities of external load, stack height, contact arc length, and deformed profile in the reversible process of loading-adhesion and unloading-delamination. Several worked examples are given as illustrations. A limiting case of adhering identical cylinders is shown to be consistent with recent model constructed by Tang et al. Such results are of particular importance in modeling the aggregation of heterogeneous carbon nanotubes or cylindrical cells, where the contacting microstructures have a different radius and/or bending stiffness.
[DOI: 10.1115/1.4000924]

Keywords: adhesion, thin shell, cylinder

1 Introduction

The adhesion of thin-walled micro- and nanoscale structures governs the functionality of many emerging technologies [1,2]. Fabrication methods in nanotechnology include adhesion-controlled manipulation and assembly of thin-walled structures such as carbon nanotube (CNT) single fibers and bundles, graphene sheets, and fullerenes [3]. Thin-film/thin-wall adhesion also controls the stability and structural integrity of flexible nanoelectronics and microtruss structures, which are subject to stiction and potential collapse under environment induced adhesion (e.g., meniscus formation at high relative humidity) [4,5]. Moreover, there has been growing interest in the role of thin-walled adhesion in biological and pathophysiological systems. Waste water treatment relies on the adhesion-controlled aggregation of bacteria, and the formation of biofilm [6] and cell-cell adhesion helps form natural and prosthetic tissues [7]. Excessive adhesion causes monocytes to bond to the aorta wall, which eventually obstructs the vessels and leads to atherosclerotic plaques [8], whereas lack of adhesion results in the loss of synaptic contacts and gives rise to Alzheimer disease [9].

Developing insights and predictive models for these systems requires an understanding of the mechanics of adhesion between thin-walled structures as a result of intersurface forces such as electrostatic, van der Waals interactions, and water meniscus. To achieve mechanical equilibrium, the adhesion energy must balance the mechanical energies due to external load and structural deformation [10]. Notwithstanding the many existing and successful solid-solid adhesion models, a new theory is needed to explicitly address adhesion between thin-walled structures that are *dissimilar* in stiffness, geometry, and dimension. Here, we consider one particular class of geometries: parallel, thin-walled cylinders with dissimilar bending rigidity and radius. The new model has the potential to be extended to other geometries, such as contacting circular plates and thin-walled spheres [11].

Existing models for solid sphere adhesion typically incorporate Hertz contact theory. Because of geometrical incompatibility, exerting an external load on two noninteracting spheres leads to a compressive stress within the contact circle. Modifications to include interfacial adhesion were later introduced by Johnson–Kendall–Roberts (JKR), Derjaguin–Muller–Toporov (DMT), and Dugdale–Barenblatt–Maugis [10]. In essence, the interfacial attraction modifies the local deformation and introduces a tensile stress around the largely compressive contact circle. Relationships between applied load, contact radius, and approach distance are verified in a wide range of materials and interfaces. The theory is further extended to the adhesion of a solid sphere with a wavy substrate [12,13], a solid cylinder with a planar substrate, and cylinders with parallel axes [14,15]. However, these models are inadequate for thin shells, in that, the shell conforms to the substrate geometry by deforming in plate-bending, membrane-stretching, or mixed bending-stretching mode such that the notion of central compression is excluded. New models are recently developed for freestanding planar circular membranes clamped at the periphery and a planar substrate in the presence of finite range intersurface attraction, though membrane deformation is constrained to membrane stretching and negligible bending [4,16–20].

Thin shell adhesion on a planar substrate has been investigated extensively with numerical methods. Seifert [21] treated lipid vesicles as shells, developed a mechanical model by balancing the adhesion energy with Helfrich's elastic bending, and constructed a self-consistent theory for bounded and unbounded vesicles. Tang et al. [22] and Glassmaker and Hui [23] constructed an elastic model for two interacting CNTs that was consistent with molecular mechanics simulation. A critical shell radius is found below which the contact remains a line: $R_{\min}=(k/\gamma)^{1/2}$, where k is the shell stiffness and γ is the adhesion energy. Adams, Pamp, and Majidi introduced the moment-discontinuity-method to analyze the adhesion of intrinsically curved plates and beams to curved substrates [24,25]. Springman and Bassani [26,27] adopted a numerical method to probe a spherical capped shell attracted to a planar substrate via a finite range Lennard-Jones potential, derived

[1]Current address: School of Engineering and Applied Sciences (SEAS), Harvard University, Cambridge, MA 02138.
[2]Corresponding author.
Contributed by the Applied Mechanics Division of ASME for publication in the JOURNAL OF APPLIED MECHANICS. Manuscript received July 2, 2009; final manuscript received October 5, 2009; published online April 14, 2010. Assoc. Editor: Anand Jagota.

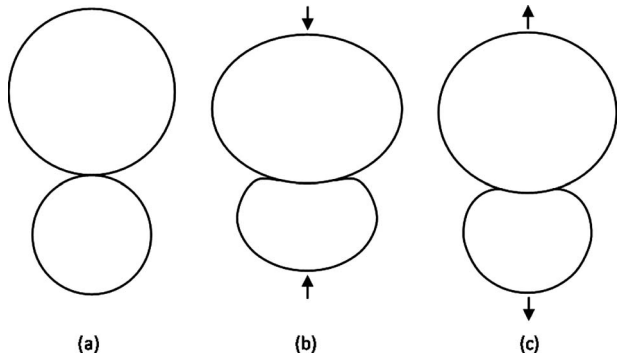

Fig. 1 Interactions between two cylindrical shells: (*a*) touching at a line contact without adhesion, (*b*) compressive deformation with adhesion, and (*c*) tensile deformation with adhesion

the "pull-in" and "pull-off" events, and further extended their model to wavy substrates under coupled chemomechanical interactions.

In this paper, we address the global deformation of two elastic cylinders with parallel axis under the following assumptions: (i) Both cylinders are hollow shells with infinite length, (ii) bending is the dominant deformation mode, and (iii) the intersurface attraction is effective at intimate contact conforming to the JKR assumption [28]. A boundary condition is introduced to represent the discontinuity in bending curvature at the contact edge. This is an extension of the moment-discontinuity-method [26,27] and is derived by minimizing the total potential energy of the system with respect to the width or radius of the contact zone. This boundary condition may also be derived using methods of fracture mechanics such as the *J*-integral [23,29] and the stress intensity factor [30]. However, in contrast to the current analysis, these derivations are beyond the scope of conventional plate and shell theory and require the evaluation of internal stress and strain fields.

2 Model

Figure 1 shows two cylinders with natural undeformed radii R_1 and R_2 being pressed into contact and then separated. Figure 2 shows the curvilinear coordinates. Upon a compressive force F, the cylinders deform to create a finite contact segment of arc length $2a$. As F becomes tensile (negative), adhesion contact remains until a critical pull-off load F_0 is reached. A spontaneous separation of the adherends follows that reduces a to zero.

Let s_1 and s_2 denote the arc lengths of the bottom and top cylinders, respectively, measured from the cylinder poles. Symmetry about the vertical axis requires the left-half of the system to be considered, and analysis is limited to $L_1=\pi R_1$ and $L_2=\pi R_2$. Define

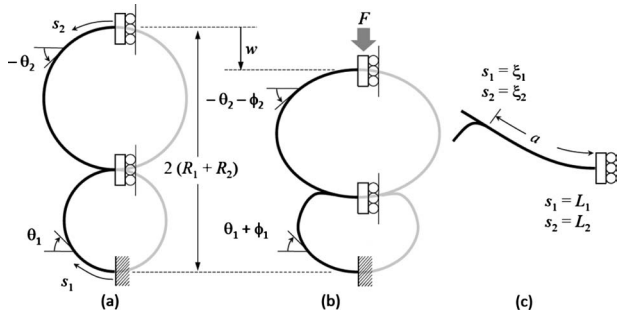

Fig. 2 Curvilinear coordinates

$$\xi_1 = L_1 - a \quad \text{and} \quad \xi_2 = L_2 - a \tag{1}$$

corresponding to the arc length at which the bottom and top cylinders make contact. In their natural configuration, the cylinders are deflected by an angle

$$\theta_1 = s_1/R_1 \quad \text{and} \quad \theta_2 = -s_2/R_2 \tag{2}$$

with respect to horizontal. Under an applied load, the deflection increases by an angle ϕ_1 and ϕ_2 such that the final deflection is $\theta_1+\phi_1$ and $\theta_2+\phi_2$.

2.1 Boundary Conditions. The angular deformations $\phi_1=\phi_1(s_1)$ and $\phi_2=\phi_2(s_2)$ and arc length a must satisfy boundary conditions that ensure both mirror symmetry about the vertical axis and geometric compatibility between the cylinders along their contact. Noting that $\theta_1(0)=\theta_2(0)=\theta_1(L_1)=\theta_2(L_2)=0$, it follows that in order for symmetry to be preserved, the boundary conditions

$$\phi_1(0) = \phi_2(0) = \phi_1(L_1) = \phi_2(L_2) = 0 \tag{3}$$

must be satisfied. To ensure geometric compatibility and to prevent interpenetration of the adhering surfaces, the two cylinders must share the same shape along the length of contact. Referring to Fig. 2(*b*), this requires $\pi-(\theta_1+\phi_1)$ to equal $-(\theta_2+\phi_2)-\pi$ for all values of $s_1 \in [\xi_1, L_1]$ and $s_2 \in [\xi_2, L_2]$, where $s_2=s_1-\xi_1+\xi_2$,

$$\theta_1(s_1) + \phi_1(s_1) = 2\pi + \theta_2(s_1 - \xi_1 + \xi_2) + \phi_2(s_1 - \xi_1 + \xi_2), \quad \forall\, s_1 \in [\xi_1, L_1] \tag{4}$$

Lastly, the deformations ϕ_1 and ϕ_2 must allow the cylinders to form a close loop such that the isoperimetric constraints $\int_0^{L_1}\cos(\theta_1+\phi_1)ds_1=\int_0^{L_2}\cos(\theta_2+\phi_2)ds_2=0$ are satisfied. In light of the compatibility condition in Eq. (4), this is equivalent to

$$\int_0^{\xi_1} \cos(\theta_1 + \phi_1)ds_1 = \int_0^{\xi_2} \cos(\theta_2 + \phi_2)ds_2 = -\int_{\xi_1}^{L_1} \cos(\theta_1 + \phi_1)ds_1 \tag{5}$$

At this point it is convenient to define

$$\phi_a = \{\phi_1 : s_1 \in [\xi_1, L_1]\} \tag{6}$$

This allows deformation to be represented by three independent functions ϕ_1, ϕ_2, and ϕ_a on the domains $[0,\xi_1]$, $[0,\xi_2]$, and $[\xi_1,L_1]$, respectively. By introducing ϕ_a, the boundary conditions reduce to

$$\phi_1(0) = \phi_2(0) = \phi_a(L_1) = 0 \tag{7}$$

$$\phi_a(\xi_1) = \phi_1(\xi_1) = 2\pi + \phi_2(\xi_2) + \theta_2(\xi_2) - \theta_1(\xi_1) \tag{8}$$

$$\int_0^{\xi_1} \cos(\theta_1 + \phi_1)ds_1 = \int_0^{\xi_2} \cos(\theta_2 + \phi_2)ds_2 = -\int_{\xi_1}^{L_1} \cos(\theta_1 + \phi_a)ds_1 \tag{9}$$

It is important to note that these conditions explicitly prevent interpenetration of the cylinders *only* along the contact zone ($s_1 \in [\xi_1, L_1]$).

2.2 Energy Functional. The cylindrical walls are treated as inextensible *elastica*. Hence, extension and shear strains are ignored and the elastic strain energy is limited to bending. Let k_1 and k_2 denote the dimensionless flexural rigidity of the bottom and top cylinders, respectively, where both k_i are normalized with respect to the flexural rigidity per unit length of cylinder 1, $D_1=E_1{h_1}^3/12(1-{\upsilon_1}^2)$, with E_1 the elastic modulus, υ_1 Poisson's ratio, and h_1 the wall thickness. The total elastic strain energy of

the system Γ can be decomposed into the segments corresponding to the domains $[0,\xi_1]$, $[0,\xi_2]$, and $[\xi_1,L_1]$ as follows:

$$\Gamma_1 = \int_0^{\xi_1} \frac{1}{2} k_1 \phi_{1,1}^2 ds_1, \quad \Gamma_2 = \int_0^{\xi_2} \frac{1}{2} k_2 \phi_{2,2}^2 ds_2$$

$$\Gamma_3 = \int_{\xi_1}^{L_1} \left\{ \frac{1}{2} k_1 \phi_{a,1}^2 + \frac{1}{2} k_2 \left(\phi_{a,1} + \frac{1}{R_1} + \frac{1}{R_2} \right)^2 \right\} ds_1 \tag{10}$$

where $\phi_{i,j} = d\phi_i / ds_j$. The total potential energy of the system Π is computed by combining these elastic strain energies with the work U_f of the external load F, the virtual work U_λ of the isoperimetric constraints in Eq. (9), and the work of adhesion $W = \gamma\, a$, with γ the interfacial adhesion energy per unit length of cylinder. That is,

$$\Pi = \Gamma_1 + \Gamma_2 + \Gamma_3 + U_f + U_\lambda - W \tag{11}$$

where

$$U_F = \int_0^{\xi_1} F \sin(\theta_1 + \phi_1) ds_1 - \int_0^{\xi_2} F \sin(\theta_2 + \phi_2) ds_2 \tag{12}$$

and

$$U_\lambda = \int_0^{\xi_1} \lambda_1 \cos(\theta_1 + \phi_1) ds_1 + \int_0^{\xi_2} \lambda_2 \cos(\theta_2 + \phi_2) ds_2 + \int_{\xi_1}^{L_1} (\lambda_1 + \lambda_2) \cos(\theta_1 + \phi_a) ds_1 \tag{13}$$

The Lagrangian multipliers λ_1 and λ_2 in Eq. (13) are unknown constants and correspond to the internal "hoop" stress at the points $s_1 = s_2 = 0$. The total potential energy of the system may be expressed by the functional

$$\begin{aligned} \Pi = & \int_0^{\xi_1} \left\{ \frac{1}{2} k_1 \phi_{1,1}^2 + F \sin(\theta_1 + \phi_1) + \lambda_1 \cos(\theta_1 + \phi_1) \right\} ds_1 \\ & + \int_0^{\xi_2} \left\{ \frac{1}{2} k_2 \phi_{2,2}^2 - F \sin(\theta_2 + \phi_2) + \lambda_2 \cos(\theta_2 + \phi_2) \right\} ds_2 \\ & + \int_{\xi_1}^{L_1} \left\{ \frac{1}{2} (k_1 + k_2) \phi_{a,1}^2 + k_2 \phi_{a,1} \left(\frac{1}{R_1} + \frac{1}{R_2} \right) + \frac{1}{2} k_2 \left(\frac{1}{R_1} + \frac{1}{R_2} \right)^2 \right. \\ & \left. + (\lambda_1 + \lambda_2) \cos(\theta_1 + \phi_a) - \gamma \right\} ds_1 \end{aligned} \tag{14}$$

3 Analysis

At equilibrium, the energy functional Π must be stationary with respect to kinematically admissible variations of the form

$$\phi_1 = \phi_1^* + \delta\phi_1, \quad \phi_2 = \phi_2^* + \delta\phi_2, \quad \phi_a = \phi_a^* + \delta\phi_a, \quad a = a^* + \delta a \tag{15}$$

Here, χ^* denotes the value of χ at equilibrium and $\delta\chi$ is an arbitrary but infinitesimally small variation from χ^*. In the subsequent analysis, it is convenient to define the Lagrangian densities

$$\Lambda_1 = \tfrac{1}{2} k_1 \phi_{1,1}^2 + F \sin(\theta_1 + \phi_1) + \lambda_1 \cos(\theta_1 + \phi_1)$$

$$\Lambda_2 = \tfrac{1}{2} k_2 \phi_{2,2}^2 - F \sin(\theta_2 + \phi_2) + \lambda_2 \cos(\theta_2 + \phi_2)$$

$$\Lambda_a = \frac{1}{2} (k_1 + k_2) \phi_{a,1}^2 + k_2 \phi_{a,1} \left(\frac{1}{R_1} + \frac{1}{R_2} \right) + \frac{1}{2} k_2 \left(\frac{1}{R_1} + \frac{1}{R_2} \right)^2 + (\lambda_1 + \lambda_2) \cos(\theta_1 + \phi_a) - \gamma \tag{16}$$

3.1 Balance Laws. Let $\delta\Pi_\phi$ denote the variation in Π induced by the first three variations in Eq. (15). Employing the calculus of variations and noting that the variations must be kinematically admissible, it is straightforward to show that $\delta\Pi_\phi$ vanishes if and only if the balance laws

$$\frac{\partial \Lambda_1}{\partial \phi_1} - \frac{d}{ds_1} \left(\frac{\partial \Lambda_1}{\partial \phi_{1,1}} \right) = 0, \quad \frac{\partial \Lambda_2}{\partial \phi_2} - \frac{d}{ds_2} \left(\frac{\partial \Lambda_2}{\partial \phi_{2,2}} \right) = 0,$$

$$\frac{\partial \Lambda_a}{\partial \phi_a} - \frac{d}{ds_1} \left(\frac{\partial \Lambda_a}{\partial \phi_{a,1}} \right) = 0 \tag{17}$$

and natural boundary condition

$$\left(\frac{\partial \Lambda_1}{\partial \phi_{1,1}} \right)_{s_1 = \xi_1} + \left(\frac{\partial \Lambda_2}{\partial \phi_{2,2}} \right)_{s_2 = \xi_2} - \left(\frac{\partial \Lambda_a}{\partial \phi_{a,1}} \right)_{s_1 = \xi_1} = 0 \tag{18}$$

are satisfied (see Appendix A for derivation). Equation (17) corresponds to the differential form of the moment balance along the segments $s_1 \in [0,\xi_1]$, $s_2 \in [0,\xi_2]$, and $s_1 \in [\xi_1, L_1]$, respectively, while Eq. (18) corresponds to the moment balance at the edge of the interface ($s_1 = \xi_1$).

Substituting the Lagrangian densities into Eq. (17) results in a system of three second-order ordinary differential equations. Solving these will introduce six constants of integration $(c_1, c_2, \ldots, c_6)$, resulting in altogether nine unknowns: $a, \lambda_1, \lambda_2, c_1, c_2, \ldots, c_6$. However, so far, we have presented only eight linearly independent equations: the five boundary conditions in Eqs. (7) and (8), the two isoperimetric constraints in Eq. (9), and moment balance (18) at $s_1 = \xi_1$ and $s_2 = \xi_2$. In order to calculate the unknown constants, a ninth linearly independent equation is required. This is furnished by the fourth variation in Eq. (15) and is presented in Sec. 3.2.

3.2 Jump Condition. The fourth variation in Eq. (15) results in a variation of the potential energy that has the form $\delta\Pi_a = (d\Pi/da)\delta a$. Since δa is arbitrary, $\delta\Pi_a$ vanishes if and only if $d\Pi/da = 0$. Employing Leibniz' integration rule, the chain rule, the balance laws in Eq. (17), and the natural boundary condition in Eq. (18), it follows that $d\Pi/da = 0$ reduces to

$$\begin{aligned} & (\Lambda_a)_{s_1=\xi_1} - (\Lambda_1)_{s_1=\xi_1} - (\Lambda_2)_{s_2=\xi_2} + \left(\frac{\partial \Lambda_1}{\partial \phi_{1,1}} \right)_{s_1=\xi_1} \{ \phi_{1,1}(\xi_1) - \phi_{a,1}(\xi_1) \} \\ & + \left(\frac{\partial \Lambda_2}{\partial \phi_{2,2}} \right)_{s_2=\xi_2} \left\{ \phi_{2,2}(\xi_2) - \phi_{a,1}(\xi_1) - \frac{1}{R_1} - \frac{1}{R_2} \right\} = 0 \end{aligned} \tag{19}$$

Details of the derivation are provided in Appendix B. Jump condition (19) provides the ninth equation necessary to complete the system of linear equations needed to solve for the nine unknown constants: $a, \lambda_1, \lambda_2, c_1, c_2, \ldots, c_6$. Physically, Eq. (19) corresponds to the balance of the work of adhesion with the elastic energy release rate associated with variations of the arc length a from its value at equilibrium.

3.3 Solution. The governing equations are derived by substituting the expressions for Λ_1, Λ_2, and Λ_a into the above equations. A solution can easily be obtained by linearizing for small ϕ_1 and ϕ_2. This yields the following set of governing equations (see Appendix C):

$$k_1 \phi_{1,11} = F \cos(\theta_1) - \lambda_1 \sin(\theta_1) \tag{20}$$

$$k_2 \phi_{2,22} = -F \cos(\theta_2) - \lambda_2 \sin(\theta_2) \tag{21}$$

$$(k_1 + k_2) \phi_{a,11} = -(\lambda_1 + \lambda_2) \sin(\theta_1) \tag{22}$$

Also, natural boundary condition (18) and jump condition (19) imply

$$k_1\{\phi_{1,1}(\xi_1) - \phi_{a,1}(\xi_1)\}k_2\left\{\phi_{2,2}(\xi_2) - \phi_{a,1}(\xi_1) - \frac{1}{R_1} - \frac{1}{R_2}\right\} = 0 \tag{23}$$

and

$$\frac{1}{2}k_1\{\phi_{1,1}(\xi_1) - \phi_{a,1}(\xi_1)\}^2 + \frac{1}{2}k_2\left\{\phi_{2,2}(\xi_2) - \phi_{a,1}(\xi_1) - \frac{1}{R_1} - \frac{1}{R_2}\right\}^2 = \gamma \tag{24}$$

respectively. As before, the kinematic boundary conditions are

$$\phi_1(0) = \phi_2(0) = \phi_a(L_1) = 0 \tag{25}$$

$$\phi_a(\xi_1) = \phi_1(\xi_1) = 2\pi + \phi_2(\xi_2) + \theta_2(\xi_2) - \theta_1(\xi_1) \tag{26}$$

Lastly, linearization reduces the isoperimetric constraints to

$$\int_0^{\xi_1}\{\cos(\theta_1) - \phi_1\sin(\theta_1)\}ds_1 = \int_0^{\xi_2}\{\cos(\theta_2) - \phi_2\sin(\theta_2)\}ds_2 = -\int_{\xi_1}^{L_1}\{\cos(\theta_1) - \phi_a\sin(\theta_1)\}ds_1 \tag{27}$$

Solving balance equations (20)–(22) yields six constants of integration, $c_1, c_2, \ldots, c_6$. Hence, there are altogether nine unknowns: $a, \lambda_1, \lambda_2, c_1, c_2, \ldots, c_6$, to be determined by substituting the solutions to Eqs. (20)–(22) into Eqs. (23)–(27). Consequently, there is a system of nine equations with nine unknowns.

Numerical solutions to the system described in Eqs. (20)–(27) are presented in Figs. 3–5. In all three sets of figures, (a) depicts the deformation under a varying compressive load F, (b) the contact length a as a function of F, and (c) F as a function of the compression distance w. The results in (b) and (c) are provided for various values of the adhesion energy γ. Here, the compression distance, or the change in height of the stacked cylinders (equilibrium stack height minus the sum of undeformed cylinders) w, is defined as

$$w = 2(R_1 + R_2) - \int_0^{\xi_1}\sin(\theta_1 + \phi_1)ds_1 + \int_0^{\xi_2}\sin(\theta_2 + \phi_2)ds_2 \tag{28}$$

The input parameters $(k_1, k_2, R_1, R_2, \gamma, F)$ and calculated values (a, w) are all unitless.

4 Worked Examples

The governing equations are derived using the principle of minimum potential energy. The potential energy functional comprises the strain energy created by elastic bending in both the contacting and noncontacting portions of the cylinders, the potential energy of the external load F, and the work of adhesion to expose new surfaces. Apart from the standard differential and boundary forms of moment balance (17) and (18), stationarity of the potential energy functional furnishes a jump condition at the edge $(s_1 = \xi_1, s_2 = \xi_2)$ of contact zone (19). A simpler jump condition had previously been derived for adhesion of a single cylinder to a rigid, flat substrate, a result that has recently been shown to be equivalent to a discontinuity in the internal moment [31]. The jump condition in Eq. (19), however, has more terms since it concerns adhesion between two generally dissimilar thin-walled cylinders. Moreover, it does not appear to correspond to a discontinuity in internal moment and is instead related to a discontinuity in material (configurational) forces or Eshelbian energy-momentum.

4.1 Same Stiffness and Radii ($k_1 = k_2, R_1 = R_2$) . Figure 3(*a*) shows the deformed cylinders with $k_1 = k_2 = 1$ and $R_1 = R_2 = 1$, under the coupled action of an external compressive load and adhesion with $\gamma = 3$. Both cylinders are flattened at their contact interface and globally deformed to a pseudo-elliptic geometry, with the lower pole of the bottom cylinder as the reference $(s_1 = 0)$. The deformation is symmetric with respect to the planar contact. In this respect, the identical cylinders deform in a manner qualita-

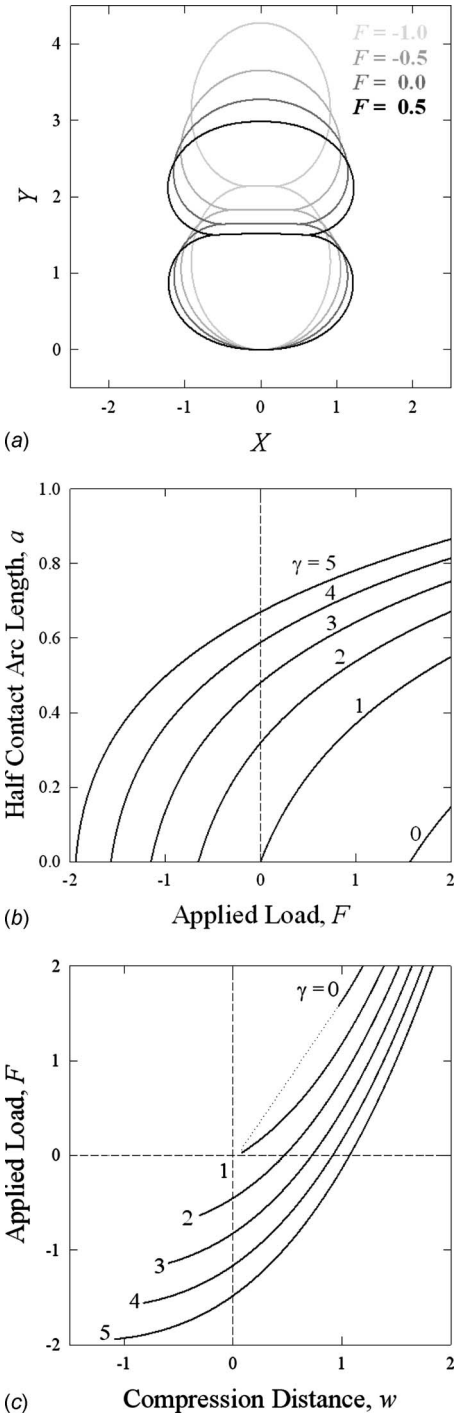

Fig. 3 Adhesion between two identical cylindrical shells with the same bending stiffness ($k_1 = k_2 = 1$) and radii ($R_1 = R_2 = 1$) under a compressive load F for $\gamma = 3$ (unless indicated otherwise). (*a*) Deformed profile with pole of bottom cylinder as reference. (*b*) Half contact arc length as a function of compressive load. (*c*) Compressive load F as a function of compression distance w, with the dashed line indicating line contact ($a = 0$) where adhesion has no influence on the interacting cylinders.

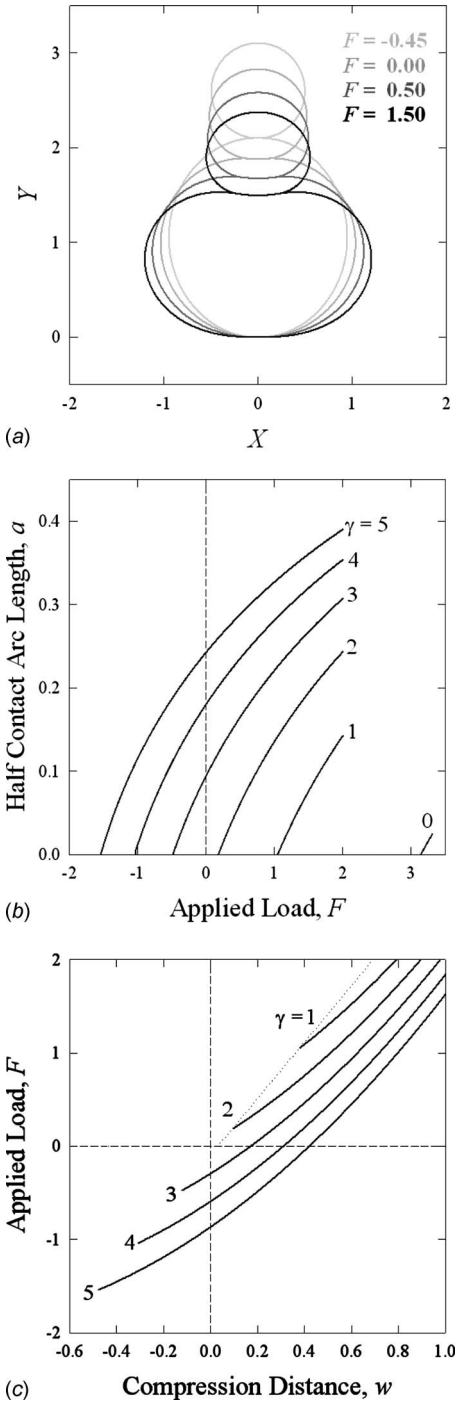

Fig. 4 Adhesion between two cylindrical shells with the same bending stiffness ($k_1=k_2=1$) but different radii ($R_1=1, R_2=0.5$) under a compressive load F for $\gamma=3$ (unless indicated otherwise). (*a*) Deformed profile. (*b*) Half contact arc length as a function of compressive load. (*c*) Compressive load F as a function of compression distance w, with the dashed line indicating line contact ($a=0$) where adhesion has no influence.

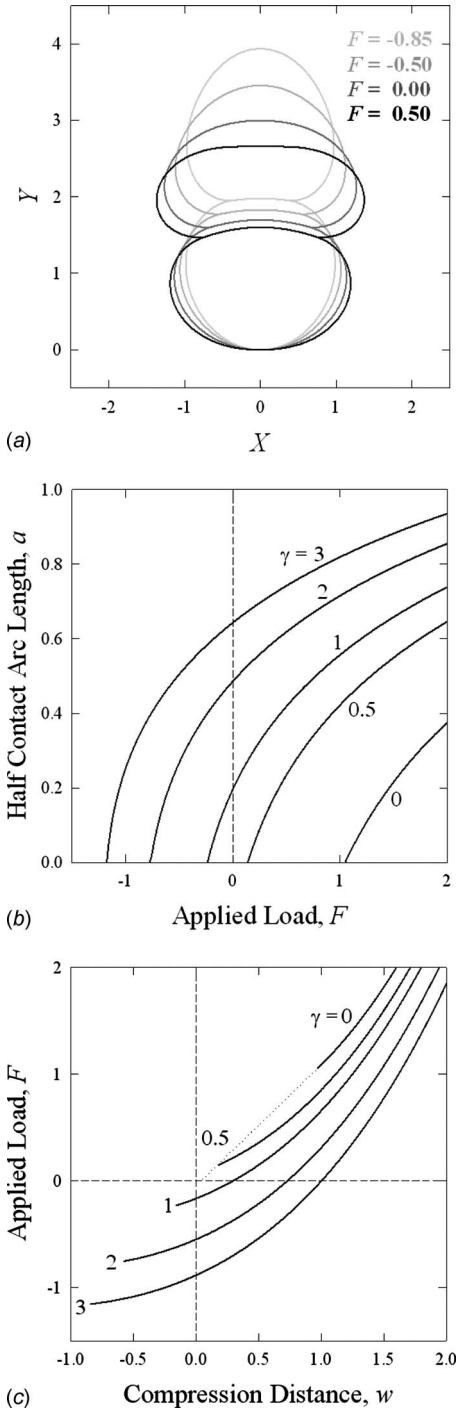

Fig. 5 Adhesion between two cylindrical shells with the same radii ($R_1=R_2=1$) but different bending stiffnesses ($k_1=1, k_2=0.5$) under a compressive load F for $\gamma=3$ (unless indicated otherwise). (*a*) Deformed profile. (*b*) Half arc contact length as a function of compressive load. (*c*) Compressive load F as a function of compression distance w, with the dashed line indicating line contact ($a=0$) where adhesion has no influence.

tively similar (but not equivalent) to the adhesion of a single cylinder to a flat, rigid substrate. Figures 3(*b*) and 3(*c*) show the mechanical responses $a(F)$ and $F(w)$ for a range of γ. As F decreases, the contact shrinks and continues to be finite even when the external load turns tensile ($F<0$). When the tensile load reaches the threshold, $F_0=\min(F)$, the contact vanishes ($a=0$) and the two adhering cylinders snap, leading to pull-off. The critical tensile load (negative F) increases with increasing γ; e.g., $F_0(\gamma=3)\approx-1.1$ and $F_0(\gamma=5)=-2$. Interestingly, $F_0(\gamma=1)=0$ is predicted, implying that the work of adhesion is insufficient to cause spontaneous adhesion of the two cylinders. A minimum compressive load is necessary to make finite contact ($a>0$). In reality, adhesion is the result of intersurface forces with *finite* range such that the cylinders interact even in the absence of intimate contact

and a tensile load is always needed to separate the adherends. For $0<\gamma<1$, F_0 is positive at $a=0$ such that adhesion is irrelevant for $0<F<F_0$ and Π thus comprises the elastic deformation energy and potential energy due to external load only. Physically, when F falls below F_0, the contact area remains a line ($a=0$) until w reduces to zero. There exists a minimal critical cylinder radius $R_{\min}$, below which the contact is always zero (to be discussed in Sec. 5). In Fig. 3(*c*), the compression distance is always positive ($w>0$) even in the absence of external load ($F=0$) as adhesion compels the two cylinders. As the load turns tensile ($F<0$), w reduces further and the cylinder becomes more elongated about the vertical axis until pull-off occurs at the termini of all curves.

4.2 Same Stiffness and Different Radii ($k_1=k_2, R_1=2R_2$) . Figure 4(*a*) shows two dissimilar cylinders with $k_1=k_2=1$ but $R_1=1$ and $R_2=0.5$. Here, the deformation about the curved contact becomes asymmetric. Elastic deformation is mainly confined to the larger cylinder even along the contact length. The relations $a(F)$ and $F(w)$ are similar to Figs. 3(*b*) and 3(*c*) despite a shift in F_0. The $F(w)$ for $\gamma=1$ and 2 terminate as adhesion loses its influence on the cylinders.

4.3 Different Stiffness and Same Radii ($k_1=2k_2, R_1=R_2$) . Figure 5(*a*) shows dissimilar cylinders with $k_1=1$ and $k_2=0.5$, but $R_1=R_2=1$. The more compliant cylinder suffers from a larger degree of deformation. For $F=1$, the change in angle ϕ_2 is as large as 0.6 rad over much of the noncontacting portion. Hence, the small angle approximation used to derive Eqs. (20)–(22) and (27) is no longer suitable and the exact differential equation or higher order approximation is necessary. Moreover, because of the greater compliance, Figs. 5(*b*) and 5(*c*) are limited to $\gamma\leq 3$. For larger γ, the more compliant cylinder will spontaneously adhere to the stiffer cylinder and undergo deformation angles ϕ_2 that are well beyond the range of the small angle approximation.

4.4 Example of Carbon Nanotubes. A practical example is the mechanical deformation of CNT in the presence of adhesion. Though the proper computation should incorporate the crystallographic structure and orientation, we adopt the present continuum model and compare the results with molecular simulation by Tang et al. [22]. A comprehensive summary of published CNT materials parameters is given by Tu and Ou-Yang [25]. According to Sears and Batra [32], an equivalent elastic tube representation of CNT possesses sheet thickness $h=0.1$ nm, radius $R=0.6$ nm, and elastic modulus $E=3.0$ TPa. In order to achieve a contact arc length $a=0.1$ nm (17% of R), an adhesion energy of $\gamma\approx 1.0$ J m^{-2} is required, which is a reasonable estimate of the van der Waals interactions. In the presence of water meniscus alone, $\gamma\approx 0.144$ J m^{-2}, which falls below the critical adhesion energy γ^*, the contact area is a line ($a=0$), and the corresponding pull-off load vanishes ($F_0=0$).

5 Discussion

It is worthwhile to compare the present model with the classical JKR and DMT models for adhering solid spheres. For example, the predicted pull-off force F_0 is found to have a much stronger dependence on the size (R) than stiffness (k), in reminiscence of $(F_0)_{\mathrm{JKR}}=(3/2)\pi R\gamma$ and $(F_0)_{\mathrm{DMT}}=\pi R\gamma$, where both depend only on the solid sphere dimension but not on materials stiffness. To make a rigorous comparison, the pull-off force is normalized by $\pi R_{\mathrm{eff}}\gamma$ with $R_{\mathrm{eff}}{}^{-1}=R_1{}^{-1}+R_2{}^{-1}$ being the effective cylinder radius. Figure 6(*a*) presents $R_1=R_2=1$ and $k_1=1$ for a range of k_2. In the limit of large γ, $F_0/\pi R\gamma$ approaches an asymptote of approximately 1/4, independent of k_1 and k_2. On the other hand, once the adhesion energy falls below a threshold of γ^*, pull-off occurs at $F_0(\gamma\leq\gamma^*)=0$. Despite the similarity with JKR, cylindrical shells deviate significantly at small γ. Figure 6(*b*) shows $k_1=k_2=1$ and $R_1=1$ for a range of R_2. The monotonic increasing F_0 again shows

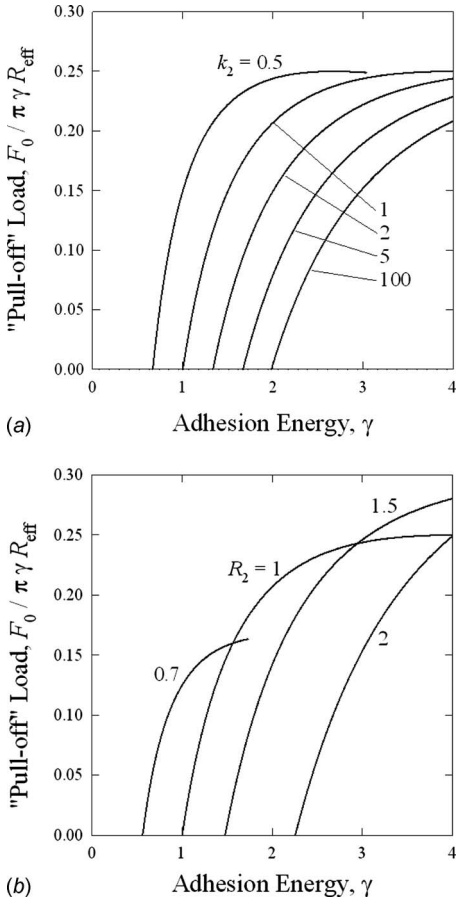

Fig. 6 Normalized pull-off strength F_0 as a function of adhesion energy γ. (*a*) Same radius ($R_1=R_2=1$), but different stiffness with $k_1=1$. (*b*) Same stiffness ($k_1=k_2=1$), but different radii with $R_1=1$.

a minimum threshold with $F_0(\gamma\leq\gamma^*)=0$, but there does not exist a common asymptote for large γ. The fact that the upper limit for each $F_0(\gamma)$ curve decreases with increasing R_2 indicates that (i) the larger cylinder becomes more compliant and thus requires a smaller pull-off force, and (ii) the pull-off depends predominantly on the cylinder dimension alluding to the JKR model.

A fundamental difference between the current model and JKR is noted. A distinct feature of the JKR is the local deformation of the adhering spheres at the contact circle. In essence, the combined applied load and adhesion force press a sphere against a rigid planar substrate to create a Hertz contact circle. While retaining the contact circle, the adhesion force is then removed and replaced with a local deformation around the contact circle. This is done by assuming that a circular punch in full contact with a half elastic continuum pulls on the substrate giving rise to a linear "relaxation" and reduction in the approach displacement. Proper energy balance thus leads to a mechanical instability or pull-off at a critical tensile applied load and a nonzero contact radius. Should the essential relaxation be ignored, the contact circle always shrinks to zero (one-point contact) at pull-off. In general, the characteristic nonzero pull-off contact is expected in geometrically incompatible surfaces (e.g., spheres). Existing models for thin-walled vesicles ignore local deformation and indeed predict zero pull-off radius [33–35], though it must be emphasized that determination of the exact pull-off radius proves to be quite elusive. Nevertheless, our present model does not consider local deformation and the contact arc length must therefore reduce to zero (i.e., line contact) at pull-off. A comprehensive model is beyond the scope of this paper.

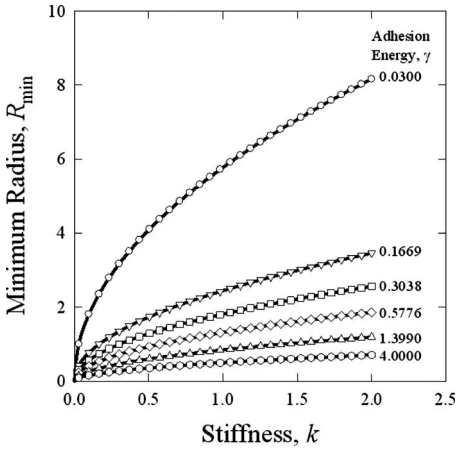

Fig. 7 Threshold radius for line contact ($a=0$) as function of stiffness and adhesion energy. ($R_{min}=(k/\gamma)^{1/2}$ for $R_1=R_2=R$ and $k_1=k_2=k$.)

The eccentric behavior of line contact ($a=0$) present at small compressive external load (cf. Fig. 3(*c*)) is worth discussing. Based on the assumption that carbon nanotubes are planar graphene sheets folded into a cylindrical shell, Hui and co-workers [22,23] used an alternative method to derive a minimum cylindrical radius below which the adhesion contact remains a line: $R_{min}=(k/\gamma)^{1/2}$ for $R_1=R_2=R$ and $k_1=k_2=k$. Compliant cylinders (small k) coupled with strong adhesion (large γ) is more prone to deformation and thus a small R_{min}. The present model considers cylinders that are initially stress-free. To deduce the relation between R_{min}, k, and γ, values of R and k are randomly chosen, and the relation $a(F)$ is then found for a range of γ. The unique curve intersecting the origin ($a=0$ and $F=0$) corresponds to the value of $\gamma(R_{min})$. For instance, in Fig. 3(*b*), $k=1$ and $R_{min}=1$; therefore, $\gamma=1$ because the corresponding $a(F)$ intersects the origin. The numerical routine is repeated for a range of k and R combinations. Notwithstanding the distinctly different assumptions and analyses in the two models, an excellent comparison between our present model (data) and that of Hui and co-workers (curves) is shown in Fig. 7 for R_{min} as a function of k for specific γ. The consistency is expected because no matter the cylinders possess an intrinsic stress, mechanical deformation to form the planar contact area causes a compressive stress to build up within the contact and immediately without, and thus raises the elastic energy of the system from the ground state of undeformed geometry. The current model is more general in the sense that dissimilar cylinders with different stiffnesses and dimensions are considered. Moreover, we deduce that the nonzero R_{min} is a consequence of the global deformation of the cylinders and the local deformation within the contact arc length, instead of "a residual stress that increases the stiffness of smaller diameter tubes" [22].

Our present 2D cylindrical shell model sheds light on the adhesion of 3D structures. One application is in cell aggregation, which is related to the formation and growth of natural, prosthetic, and malignant tissues. The existing model in literature treats cells as deformable solid spheres conforming to JKR theory. When these free entities come into contact due to thermal collision and vibration, interfacial adhesion occurs, followed by aggregation and coagulation. It is again emphasized that cells are not solid spheres but a viscoelastic cytoplasm encapsulated by a thin lipid bilayer membrane (shell). The present adhesion model properly addresses the nature of coupled shell deformation and adhesion, provides the constitutive relations between F, w, and a, and thus yields the basis for a correct statistical portrayal of the Gibbs free energy and partition function of the grand canonical ensemble [36]. Immediate biomedical application is found in deriving the physical thresholds for cell aggregation (e.g., concentration, dimension, and temperature). Long-range surface forces can also be incorporated into the present model such that the adhering surfaces sense the presence of their counterpart even prior to direct contact, as shown in our latest work for freestanding membrane clamped at the periphery adhering to a planar substrate [20].

6 Conclusion

Using an energy balance, we derived the adhesion mechanics for two interacting elastic cylindrical shells with ranges of bending stiffness, radii, and adhesion energy. Relationships are established between the measurable quantities at equilibrium, namely, applied load, stack height, contact length and deformed cylinder profiles, and the quasistatic adhesion-delamination trajectories. The graphs and trends presented have significant implications in the adhesion of similar and dissimilar interfaces in micro-/nanoshell structures. Such interactions are relevant to a variety of systems in nanoscience and technology, life-sciences, and tissue engineering.

Acknowledgment

The authors are grateful to the reviewers and the associate editor, Dr. Anand Jagota, for many invaluable suggestions. K.-T.W. is supported by the National Science Foundation CMMI No. 0757140.

Appendix A

Following the definitions in Eqs. (14) and (16), the total potential energy of the system may be expressed as

$$\Pi=\int_0^{\xi_1}\Lambda_1 ds_1+\int_0^{\xi_2}\Lambda_2 ds_2+\int_{\xi_1}^{L_1}\Lambda_a ds_1 \tag{A1}$$

At equilibrium, Π must be stationary with respect to variations in ϕ_1, ϕ_2, and ϕ_a as well as their derivatives ($\phi_{1,1}$, $\phi_{2,2}$, and $\phi_{a,1}$). Applying these variations simultaneously to Π yields an expression of the form

$$\delta\Pi_\phi=\int_0^{\xi_1}\left\{\frac{\partial\Lambda_1}{\partial\phi_1}\delta\phi_1+\frac{\partial\Lambda_1}{\partial\phi_{1,1}}\delta\phi_{1,1}\right\}ds_1+\int_0^{\xi_2}\left\{\frac{\partial\Lambda_2}{\partial\phi_2}\delta\phi_2+\frac{\partial\Lambda_2}{\partial\phi_{2,2}}\delta\phi_{2,2}\right\}ds_2+\int_{\xi_1}^{L_1}\left\{\frac{\partial\Lambda_a}{\partial\phi_a}\delta\phi_a+\frac{\partial\Lambda_a}{\partial\phi_{a,1}}\delta\phi_{a,1}\right\}ds_1 \tag{A2}$$

By the chain rule,

$$\begin{aligned}\int_0^{\xi_1}\left\{\frac{\partial\Lambda_1}{\partial\phi_{1,1}}\delta\phi_{1,1}\right\}ds_1&=\int_0^{\xi_1}\left\{\frac{d}{ds}\left(\frac{\partial\Lambda_1}{\partial\phi_{1,1}}\delta\phi_1\right)-\frac{d}{ds}\left(\frac{\partial\Lambda_1}{\partial\phi_{1,1}}\right)\delta\phi_1\right\}ds_1\\&=\left(\frac{\partial\Lambda_1}{\partial\phi_{1,1}}\delta\phi_1\right)_{s_1=\xi_1}-\left(\frac{\partial\Lambda_1}{\partial\phi_{1,1}}\delta\phi_1\right)_{s_1=0}-\int_0^{\xi_1}\left\{\frac{d}{ds}\left(\frac{\partial\Lambda_1}{\partial\phi_{1,1}}\right)\delta\phi_1\right\}ds_1\end{aligned} \tag{A3}$$

Here, the operation $(f)_{x=y}$ denotes the value of f at $x=y$. Applying this same identity to the other integrals in Eq. (A2),

$$\delta\Pi_\phi = \left(\frac{\partial\Lambda_1}{\partial\phi_{1,1}}\delta\phi_1\right)_{s_1=\xi_1} - \left(\frac{\partial\Lambda_1}{\partial\phi_{1,1}}\delta\phi_1\right)_{s_1=0} + \int_0^{\xi_1}\left\{\frac{\partial\Lambda_1}{\partial\phi_1} - \frac{d}{ds}\left(\frac{\partial\Lambda_1}{\partial\phi_{1,1}}\right)\right\}\delta\phi_1 ds_1 \left(\frac{\partial\Lambda_2}{\partial\phi_{2,2}}\delta\phi_2\right)_{s_2=\xi_2} - \left(\frac{\partial\Lambda_2}{\partial\phi_{2,2}}\delta\phi_2\right)_{s_2=0} + \int_0^{\xi_2}\left\{\frac{\partial\Lambda_2}{\partial\phi_2} - \frac{d}{ds}\left(\frac{\partial\Lambda_2}{\partial\phi_{2,2}}\right)\right\}\delta\phi_2 ds_2 \left(\frac{\partial\Lambda_a}{\partial\phi_{a,1}}\delta\phi_a\right)_{s_1=L_1} - \left(\frac{\partial\Lambda_a}{\partial\phi_{a,1}}\delta\phi_a\right)_{s_1=\xi_1} + \int_{\xi_1}^{L_1}\left\{\frac{\partial\Lambda_a}{\partial\phi_a} - \frac{d}{ds}\left(\frac{\partial\Lambda_a}{\partial\phi_{a,1}}\right)\right\}\delta\phi_a ds_1 \tag{A4}$$

At equilibrium, $\delta\Pi_\phi$ must vanish for *kinematically admissible* variations in ϕ_1, ϕ_2, and ϕ_a.

According to the boundary conditions in Eq. (7), both $\phi_1(0) = \phi_2(0) = \phi_a(L_1) = 0$ and

$$\phi_1(0) + \delta\phi_1(0) = \phi_2(0) + \delta\phi_2(0) = \phi_a(L_1) + \delta\phi_a(L_1) = 0 \tag{A5}$$

must be satisfied. Clearly, this implies $\delta\phi_1(0) = \delta\phi_2(0) = \delta\phi_a(L_1)$; in other words, variations in the deflection ϕ_i must vanish at the points s_i where ϕ_i is prescribed. Similarly, the boundary conditions in Eq. (8) require that both the conditions

$$\phi_a(\xi_1) = \phi_1(\xi_1) = 2\pi + \phi_2(\xi_2) + \theta_2(\xi_2) - \theta_1(\xi_1) \tag{A6}$$

and

$$\phi_a(\xi_1) + \delta\phi_a(\xi_1) = \phi_1(\xi_1) + \delta\phi_1(\xi_1) = 2\pi + \phi_2(\xi_2) + \delta\phi_2(\xi_2) + \theta_2(\xi_2) - \theta_1(\xi_1) \tag{A7}$$

be satisfied. This implies $\delta\phi_a(\xi_1) = \delta\phi_1(\xi_1) = \delta\phi_2(\xi_2) = \delta\phi_\xi$. Substituting the boundary conditions expressions for $\delta\phi_i$ into Eq. (A4),

$$\delta\Pi_\phi = \left\{\left(\frac{\partial\Lambda_1}{\partial\phi_{1,1}}\right)_{s_1=\xi_1} + \left(\frac{\partial\Lambda_2}{\partial\phi_{2,2}}\right)_{s_2=\xi_2} - \left(\frac{\partial\Lambda_a}{\partial\phi_{a,1}}\right)_{s_1=\xi_1}\right\}\delta\phi_\xi + \int_0^{\xi_1}\left\{\frac{\partial\Lambda_1}{\partial\phi_1} - \frac{d}{ds}\left(\frac{\partial\Lambda_1}{\partial\phi_{1,1}}\right)\right\}\delta\phi_1 ds_1 + \int_0^{\xi_2}\left\{\frac{\partial\Lambda_2}{\partial\phi_2} - \frac{d}{ds}\left(\frac{\partial\Lambda_2}{\partial\phi_{2,2}}\right)\right\}\delta\phi_2 ds_2 + \int_{\xi_1}^{L_1}\left\{\frac{\partial\Lambda_a}{\partial\phi_a} - \frac{d}{ds}\left(\frac{\partial\Lambda_a}{\partial\phi_{a,1}}\right)\right\}\delta\phi_a ds_1 \tag{A8}$$

At this point, the variations $\delta\phi_\xi$, $\delta\phi_1$, $\delta\phi_2$, and $\delta\phi_a$ are all independent and arbitrary. Hence, in order for $\delta\Pi_\phi$ to vanish, the conditions

$$\frac{\partial\Lambda_1}{\partial\phi_1} - \frac{d}{ds_1}\left(\frac{\partial\Lambda_1}{\partial\phi_{1,1}}\right) = 0, \quad \frac{\partial\Lambda_2}{\partial\phi_2} - \frac{d}{ds_2}\left(\frac{\partial\Lambda_2}{\partial\phi_{2,2}}\right) = 0, \quad \frac{\partial\Lambda_a}{\partial\phi_a} - \frac{d}{ds_1}\left(\frac{\partial\Lambda_a}{\partial\phi_{a,1}}\right) = 0 \tag{A9}$$

$$\left(\frac{\partial\Lambda_1}{\partial\phi_{1,1}}\right)_{s_1=\xi_1} + \left(\frac{\partial\Lambda_2}{\partial\phi_{2,2}}\right)_{s_2=\xi_2} - \left(\frac{\partial\Lambda_a}{\partial\phi_{a,1}}\right)_{s_1=\xi_1} = 0 \tag{A10}$$

must be satisfied. It is important to note that boundary condition (A10) results from simultaneously applying the first three variations in Eq. (15). This is necessary since the variations are not independent, but related through the boundary conditions (7) and (8). Failure to incorporate these conditions into the calculus of variations would either eliminate kinematic constraints or introduce nonexistent ones.

Appendix B

At equilibrium, Π must be stationary with respect to variations in a. Since δa is arbitrary, the corresponding variation in Π, $\delta\Pi_a = (d\Pi/da)\delta a$, vanishes if and only if $d\Pi/da = 0$. Since both ξ_1 and ξ_2 depend on a, $d\Pi/da$ must be evaluated using Leibniz' integration rule

$$\frac{d\Pi}{da} = (\Lambda_1)_{s_1=\xi_1}\frac{d\xi_1}{da} + (\Lambda_2)_{s_2=\xi_2}\frac{d\xi_2}{da} - (\Lambda_a)_{s_1=\xi_1}\frac{d\xi_1}{da} + \int_0^{\xi_1}\left\{\frac{\partial\Lambda_1}{\partial\phi_1}\frac{d\phi_1}{da} + \frac{\partial\Lambda_1}{\partial\phi_{1,1}}\frac{d\phi_{1,1}}{da}\right\}ds_1 + \int_0^{\xi_2}\left\{\frac{\partial\Lambda_2}{\partial\phi_2}\frac{d\phi_2}{da} + \frac{\partial\Lambda_2}{\partial\phi_{2,2}}\frac{d\phi_{2,2}}{da}\right\}ds_2 + \int_{\xi_1}^{L_1}\left\{\frac{\partial\Lambda_a}{\partial\phi_a}\frac{d\phi_a}{da} + \frac{\partial\Lambda_a}{\partial\phi_{a,1}}\frac{d\phi_{a,1}}{da}\right\}ds_1 \tag{B1}$$

In light of the balance law (17),

$$\int_0^{\xi_1}\left\{\frac{\partial\Lambda_1}{\partial\phi_1}\frac{d\phi_1}{da} + \frac{\partial\Lambda_1}{\partial\phi_{1,1}}\frac{d\phi_{1,1}}{da}\right\}ds_1 = \int_0^{\xi_1}\left\{\frac{d}{ds_1}\left(\frac{\partial\Lambda_1}{\partial\phi_{1,1}}\right)\frac{d\phi_1}{da} + \frac{\partial\Lambda_1}{\partial\phi_{1,1}}\frac{d\phi_{1,1}}{da}\right\}ds_1 = \int_0^{\xi_1}\frac{d}{ds_1}\left\{\frac{\partial\Lambda_1}{\partial\phi_{1,1}}\frac{d\phi_1}{da}\right\}ds_1 = \left(\frac{\partial\Lambda_1}{\partial\phi_{1,1}}\frac{d\phi_1}{da}\right)_{s_1=\xi_1} - \left(\frac{\partial\Lambda_1}{\partial\phi_{1,1}}\frac{d\phi_1}{da}\right)_{s_1=0} \tag{B2}$$

Applying this identity to the other two integrals in Eq. (B1) and noting that $d\xi_1/da = d\xi_2/da = -1$,

$$\frac{d\Pi}{da} = (\Lambda_a)_{s_1=\xi_1} - (\Lambda_1)_{s_1=\xi_1} - (\Lambda_2)_{s_2=\xi_2} + \left(\frac{\partial\Lambda_1}{\partial\phi_{1,1}}\frac{d\phi_1}{da}\right)_{s_1=\xi_1} - \left(\frac{\partial\Lambda_1}{\partial\phi_{1,1}}\frac{d\phi_1}{da}\right)_{s_1=0} + \left(\frac{\partial\Lambda_2}{\partial\phi_{2,2}}\frac{d\phi_2}{da}\right)_{s_2=\xi_2} - \left(\frac{\partial\Lambda_2}{\partial\phi_{2,2}}\frac{d\phi_2}{da}\right)_{s_2=0} + \left(\frac{\partial\Lambda_a}{\partial\phi_{a,1}}\frac{d\phi_a}{da}\right)_{s_1=L} - \left(\frac{\partial\Lambda_a}{\partial\phi_{a,1}}\frac{d\phi_a}{da}\right)_{s_1=\xi_1} \tag{B3}$$

Next, by natural boundary condition (18), $d\Pi/da$ reduces to

$$\frac{d\Pi}{da} = (\Lambda_a)_{s_1=\xi_1} - (\Lambda_1)_{s_1=\xi_1} - (\Lambda_2)_{s_2=\xi_2} + \left\{\frac{\partial\Lambda_1}{\partial\phi_{1,1}}\left(\frac{d\phi_1}{da} - \frac{d\phi_a}{da}\right)\right\}_{s_1=\xi_1} - \left(\frac{\partial\Lambda_1}{\partial\phi_{1,1}}\frac{d\phi_1}{da}\right)_{s_1=0} + \left(\frac{\partial\Lambda_2}{\partial\phi_{2,2}}\right)_{s_2=\xi_2}\left\{\left(\frac{d\phi_2}{da}\right)_{s_2=\xi_2} - \left(\frac{d\phi_a}{da}\right)_{s_1=\xi_1}\right\} - \left(\frac{\partial\Lambda_2}{\partial\phi_{2,2}}\frac{d\phi_2}{da}\right)_{s_2=0} + \left(\frac{\partial\Lambda_a}{\partial\phi_{a,1}}\frac{d\phi_a}{da}\right)_{s_1=L_1} \tag{B4}$$

Equation (B4) represents the general expression for $d\Pi/da$ at equilibrium. It can be further simplified by applying the boundary conditions in Eqs. (7) and (8), which restrict not only ϕ_1, ϕ_2, and ϕ_a, but also their derivatives with respect to a. According to Eq. (7), ϕ_1, ϕ_2, and ϕ_a are all prescribed at $s_1 = 0$, $s_2 = 0$, and $s_1 = L_1$, respectively. Since these conditions must hold for all values of a, the derivatives $(d\phi_1/da)_{s_1=0}$, $(d\phi_2/da)_{s_2=0}$, and $(d\phi_a/da)_{s_1=L_1}$ must equal zero. This is equivalent to the condition in the calculus of variations that the variation of prescribed end points must vanish.

In contrast, $(d\phi_1/da)_{s_1=\xi_1}$, $(d\phi_2/da)_{s_2=\xi_2}$, and $(d\phi_a/da)_{s_1=\xi_1}$ are nonzero and must be computed using the boundary conditions in Eq. (8). According to Eq. (15) and the fundamental theorem of calculus,

$$\phi_1(\xi_1) = \phi_1^*(\xi_1) + \delta\phi_1(\xi_1) = \phi_1^*(\xi_1^*) - \delta a \phi_{1,1}^*(\xi_1^*) + \delta\phi_1(\xi_1) + O(\delta a^2) \tag{B5}$$

where $\xi_1^* = L_1 - a^*$ and a^* is the value of a at equilibrium. Similarly,

$$\phi_a(\xi_1) = \phi_a^*(\xi_1^*) - \delta a \phi_{a,1}^*(\xi_1^*) + \delta\phi_a(\xi_1) + O(\delta a^2) \tag{B6}$$

which, according to boundary condition (8), must be equivalent to $\phi_1(\xi_1)$. Since δa is infinitesimally small, terms of order $O(\delta a^2)$ may be omitted and so the conditions $\phi_1(\xi_1) = \phi_a(\xi_1)$ and $\phi_1(\xi_1^*) = \phi_a(\xi_1^*)$ together imply

$$-\delta a \phi_{1,1}^*(\xi_1^*) + \delta\phi_1(\xi_1) = -\delta a \phi_{a,1}^*(\xi_1^*) + \delta\phi_a(\xi_1) \tag{B7}$$

Dividing both sides by δa, taking the limit as $\delta a \to 0$, and then rearranging terms,

$$\left(\frac{d\phi_a}{da}\right)_{s_1=\xi_1} - \left(\frac{d\phi_1}{da}\right)_{s_1=\xi_1} = \phi_{a,1}(\xi_1) - \phi_{1,1}(\xi_1) \tag{B8}$$

where the asterisk denoting the value at equilibrium is henceforth omitted. Using the same argument for $\phi_2(\xi_2)$, it follows from Eq. (8) that

$$\left(\frac{d\phi_a}{da}\right)_{s_1=\xi_1} - \left(\frac{d\phi_2}{da}\right)_{s_2=\xi_2} = \phi_{a,1}(\xi_1) - \phi_{2,2}(\xi_2) + \frac{1}{R_1} + \frac{1}{R_2} \tag{B9}$$

Substituting this into Eq. (19) and setting $d\Pi/da$ equal to zero yield the following jump condition at equilibrium:

$$(\Lambda_a)_{s_1=\xi_1} - (\Lambda_1)_{s_1=\xi_1} - (\Lambda_2)_{s_2=\xi_2} + \left(\frac{\partial\Lambda_1}{\partial\phi_{1,1}}\right)_{s_1=\xi_1}\{\phi_{1,1}(\xi_1) - \phi_{a,1}(\xi_1)\} + \left(\frac{\partial\Lambda_2}{\partial\phi_{2,2}}\right)_{s_2=\xi_2}\left\{\phi_{2,2}(\xi_2) - \phi_{a,1}(\xi_1) - \frac{1}{R_1} - \frac{1}{R_2}\right\} = 0 \tag{B10}$$

Appendix C

Assuming that the deflections ϕ_1, ϕ_2, and ϕ_a are small, the Lagrangian densities may be approximated as

$$\Lambda_1 = \tfrac{1}{2}k_1\phi_{1,1}^2 + F\{\sin(\theta_1) + \phi_1\cos(\theta_1)\} + \lambda_1\{\cos(\theta_1) - \phi_1\sin(\theta_1)\}$$

$$\Lambda_2 = \tfrac{1}{2}k_2\phi_{2,2}^2 - F\{\sin(\theta_2) + \phi_2\cos(\theta_2)\} + \lambda_2\{\cos(\theta_2) - \phi_2\sin(\theta_2)\}$$

$$\Lambda_a = \frac{1}{2}(k_1+k_2)\phi_{a,1}^2 + k_2\phi_{a,1}\left(\frac{1}{R_1}+\frac{1}{R_2}\right) + \frac{1}{2}k_2\left(\frac{1}{R_1}+\frac{1}{R_2}\right)^2 + (\lambda_1+\lambda_2)\{\cos(\theta_1) - \phi_a\sin(\theta_1)\} - \gamma \tag{C1}$$

The balance equations are obtained by substituting these expressions into the Euler–Lagrange differential equation (17). This yields

$$k_1\phi_{1,11} = F\cos(\theta_1) - \lambda_1\sin(\theta_1) \tag{C2}$$

$$k_2\phi_{2,22} = -F\cos(\theta_2) - \lambda_2\sin(\theta_2) \tag{C3}$$

$$(k_1+k_2)\phi_{a,11} = -(\lambda_1+\lambda_2)\sin(\theta_1) \tag{C4}$$

where $\phi_{i,jj} = d^2\phi_i/ds_j^2$.

References

[1] Israelachvili, J. N., 1992, *Intermolecular and Surface Forces*, 2nd ed., Academic, London.

[2] Kendall, K., 2001, *Molecular Adhesion and Its Application: The Sticky Universe*, Kluwer Academic/Plenum, New York.

[3] Zhang, M., Fang, S., Zakhidov, A. A., Lee, S. B., Aliev, A. E., Williams, C. D., Atkinson, K. R., and Baughman, R. H., 2005, "Strong, Transparent, Multifunctional, Carbon Nanotube Sheets," Science, **309**(5738), pp. 1215–1219.

[4] Wong, M.-F., Duan, G., and Wan, K.-T., 2007, "Adhesion-Delamination Mechanics of a Pre-Stressed Rectangular Film Adhered Onto a Rigid Substrate," J. Appl. Phys., **101**(2), pp. 024903.

[5] Wan, K.-T., and Kogut, L., 2005, "The Coupling Effect of Interfacial Adhesion and Tensile Residual Stress on a Thin Membrane Adhered to a Flat Punch," J. Micromech. Microeng., **15**, pp. 778–784.

[6] Burks, G. A., Velegol, S. B., Paramonova, E., Lindenmuth, B. E., Feick, J. D., and Logan, B. E., 2003, "Macroscopic and Nanoscale Measurements of the Adhesion of Bacteria With Varying Outer Layer Surface Composition," Langmuir, **19**(6), pp. 2366–2371.

[7] Alberts, B., Johnson, A., Lewis, J., Raff, M., Roberts, K., and Walter, P., 2008, *Molecular Biology of the Cell*, 5th ed., Garland, New York.

[8] Joris, I., Zand, T., Nunnari, J. J., Krolikowski, F. J., and Majno, G., 1983, "Studies on the Pathogenesis of Atherosclerosis I. Adhesion and Emigration of Mononuclear Cells in the Aorta of Hypercholesterolemic Rats," Am. J. Pathol., **113**(3), pp. 341–358.

[9] Singh, N., Talalayeva, Y., Tsiper, M., Romanov, V., Dranovsky, A., Colflesh, D., Rudamen, G., Vitek, M. P., Shen, J., Yang, X., Goldgaber, D., and Schwarzman, A. L., 2001, "The Role of Alzheimer's Disease-Related Presenilin 1 in Intercellular Adhesion," Exp. Cell Res., **263**, pp. 1–13.

[10] Maugis, D., 2000, *Contact, Adhesion and Rupture of Elastic Solids*, Springer, New York.

[11] Majidi, C., and Wan, K.-T., 2009, "Adhesion Between Similar and Dissimilar Thin-Walled Microstructures," ASME International Design and Engineering Conference, San Diego, CA, Aug. 30.

[12] Guduru, P. R., 2007, "Detachment of a Rigid Solid From an Elastic Wavy Surface: Theory," J. Mech. Phys. Solids, **55**, pp. 445–472.

[13] Guduru, P. R., and Bull, C., 2007, "Detachment of a Rigid Solid From an Elastic Wavy Surface: Experiments," J. Mech. Phys. Solids, **55**, pp. 473–488.

[14] Chaudhury, M. K., Weaver, T., Hui, C. Y., and Kramer, K. J., 1996, "Adhesive Contact of Cylinder Lens and a Flat Sheet," J. Appl. Phys., **80**(1), pp. 30–37.

[15] Johnson, K. L., and Greenwood, J. A., 2008, "A Maugis Analysis of Adhesive Line Contact," J. Phys. D: Appl. Phys., **41**, p. 155315.

[16] Wong, M.-F., Duan, G., and Wan, K.-T., 2007, "Adhesion-Delamination Mechanics of a Pre-Stressed Circular Film Adhered Onto a Rigid Substrate," J. Adhes., **83**, pp. 67–83.

[17] Wan, K.-T., 2002, "Adherence of an Axisymmetric Flat Punch Onto a Clamped Circular Plate-Transition From a Rigid Plate to a Flexible Membrane," ASME J. Appl. Mech., **69**, pp. 110–116.

[18] Wan, K.-T., and Duan, J., 2002, "Adherence of a Rectangular Flat Punch Onto a Clamped Plate-Transition From a Rigid Plate to a Flexible Membrane," ASME J. Appl. Mech., **69**, pp. 104–109.

[19] Ju, B. F., Wan, K.-T., and Liu, K. K., 2004, "Indentation of a Square Elastomeric Thin Film by a Flat-Ended Cylindrical Punch in the Presence of Long-Range Intersurface Forces," J. Appl. Phys., **96**(11), pp. 6159–6163.

[20] Wan, K.-T., and Julien, S. E., 2009, "Confined Thin Film Delamination in the Presence of Intersurface Forces With Finite Range and Magnitude," ASME J. Appl. Mech., **76**, p. 051005.

[21] Seifert, U., 1997, "Configurations of Fluid Membranes and Vesicles," Adv. Phys., **46**(1), pp. 13–137.

[22] Tang, T., Jogota, A., and Hui, C.-Y., 2005, "Adhesion Between Single-Walled Carbon Nanotube," J. Appl. Phys., **97**, p. 074304.

[23] Glassmaker, N. J., and Hui, C. Y., 2004, "Elastica Solution for a Nanotube Formed by Self-Adhesion of a Folded Thin Film," J. Appl. Phys., **96**, pp. 3429–3434.

[24] Majidi, C., and Adams, G. G., 2009, "A Simplified Formulation for Adhesion Problems With Elastic Plates," Proc. R. Soc. London, Ser. A, **465**, pp. 2217–2230.

[25] Tu, Z. C., and Ou-Yang, Z. C., 2008, "Elastic Theory of Low-Dimensional Continua and Its Applications in Bio- and Nano-Structures," J. Comput. Theor. Nanosci., **5**(4), pp. 422–448.

[26] Springman, R. M., and Bassani, J. L., 2008, "Snap Transitions in Adhesion," J. Mech. Phys. Solids, **56**(6), pp. 2358–2380.

[27] Springman, R. M., and Bassani, J. L., 2009, "Mechano-Chemical Coupling in the Adhesion of Thin-Shell Structures," J. Mech. Phys. Solids, **57**, pp. 909–931.

[28] Johnson, K. L., Kendall, K., and Roberts, A. D., 1971, "Surface Energy and the Contact of Elastic Solids," Proc. R. Soc. London, Ser. A, **324**, pp. 301–313.

[29] Rice, J. R., 1968, "A Path Independent Integral and the Approximate Analysis of Strain Concentration by Notches and Cracks," ASME J. Appl. Mech., **35**, pp. 379–386.

[30] Suo, Z., and Hutchinson, J. W., 1990, "Interface Crack Between Two Elastic Layers," Int. J. Fract., **43**, pp. 1–18.

[31] Pamp, A., and Adams, G. G., 2007, "Deformation of Bowed Silicon Chips Due to Adhesion and Applied Pressure," J. Adhes. Sci. Technol., **21**, pp. 1021–1043.

[32] Sears, A., and Batra, R. C., 2004, "Macroscopic Properties of Carbon Nanotubes From Molecular-Mechanics Simulations," Phys. Rev. B, **69**, p. 235406.
[33] Seifert, U., and Lipowsky, R., 1991, "Adhesion of Vesicles," Phys. Rev. A, **44**, pp. 1182–1202.
[34] Wan, K.-T., and Liu, K. K., 2001, "Contact Mechanics of a Thin Walled Capsule Adhered Onto a Rigid Planar Substrate," Med. Biol. Eng. Comput., **39**, pp. 605–608.
[35] Shanahan, M. E. R., 1997, "A Novel Test for the Appraisal of Solid/Solid Interfacial Interactions," J. Adhes., **63**, pp. 15–29.
[36] Landau, L. D., 1984, *Statistical Physics Course of Theoretical Physics*, Vol. 5, Butterworth-Heinemann, Oxford, UK.